Biochemistry

Article

Cite This: Biochemistry 2019, 58, 3016−3030

pubs.acs.org/biochemistry

Munc13 Is a Molecular Target of Bryostatin 1

Francisco A. Blanco,[†] Agnes Czikora,[‡] Noemi Kedei,[‡] Youngki You,[†] Gary A. Mitchell,[‡] Satyabrata Pany,[†] Anamitra Ghosh,[†,§] Peter M. Blumberg,[‡] and Joydip Das*[,†]

[†]Department of Pharmacological & Pharmaceutical Sciences, College of Pharmacy, University of Houston, Houston, Texas 77204, United States

[‡]Laboratory of Cancer Biology and Genetics, Center for Cancer Research, National Cancer Institute, National Institutes of Health, Bethesda, Maryland 20892, United States

Supporting Information

ABSTRACT: Bryostatin 1 is a natural macrolide shown to improve neuronal connections and enhance memory in mice. Its mechanism of action is largely attributed to the modulation of novel and conventional protein kinase Cs (PKCs) by binding to their regulatory C1 domains. Munc13-1 is a C1 domain-containing protein that shares common endogenous and exogenous activators with novel and conventional PKC subtypes. Given the essential role of Munc13-1 in the priming of synaptic vesicles and neuronal transmission overall, we explored the potential interaction between bryostatin 1 and Munc13-1. Our results indicate that *in vitro* bryostatin 1 binds to both the isolated C1 domain of Munc13-1 (K_i = 8.07 ± 0.90 nM) and the full-length Munc13-1 protein (K_i = 0.45 ± 0.04 nM). Furthermore, confocal microscopy and immunoblot analysis demonstrated that in intact HT22 cells bryostatin 1 mimics the actions of phorbol esters, a previously established class of Munc13-1 activators, and induces plasma membrane translocation of Munc13-1, a hallmark of its activation. Consistently, bryostatin 1 had no effect on the Munc13-1^{H567K} construct that is insensitive to phorbol esters. Effects of bryostatin 1 on the other Munc13 family members, ubMunc13-2 and bMunc13-2, resembled those of Munc13-1 for translocation. Lastly, we observed an increased level of expression of Munc13-1 following a 24 h incubation with bryostatin 1 in both HT22 and primary mouse hippocampal cells. This study characterizes Munc13-1 as a molecular target of bryostatin 1. Considering the crucial role of Munc13-1 in neuronal function, these findings provide strong support for the potential role of Munc13s in the actions of bryostatin 1.

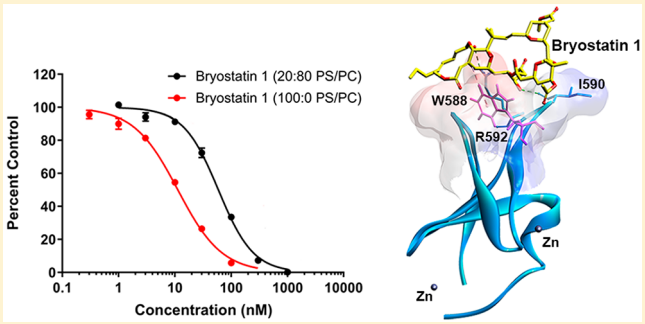

Bryostatin 1 is a natural product isolated from the marine bryozoan *Bugula neritina*.[1−3] It is a highly oxygenated macrocyclic lactone with a polyacetate backbone (Figure 1A)[1] and has been the subject of numerous clinical trials for cancer on the basis of its activity on protein kinase C (PKC).[4] More recently, preclinical studies using a mouse model for Alzheimer's disease (AD) suggested that bryostatin 1 could enhance neuronal processes. These studies found that treatments with bryostatin 1 decreased the level of oxidative stress, reduced the level of toxic protein aggregates, and augmented both the formation and maintenance of synapses.[5−7] Additionally, multiple studies highlight the potential of bryostatin 1 to improve cognitive functions through its modulation of neuronal connections.[5,8−10] Currently, the neuroprotective properties of bryostatin 1 are under study in phase II clinical trials on AD patients (Clinicaltrials.gov identifier NCT02431468).

The mechanism of action of bryostatin 1 in the central nervous system remains to be fully elucidated. However, its neuroprotective properties have been largely attributed to modulation of the PKC enzyme.[5,11] PKCs are serine-threonine kinases that dictate numerous cellular pathways, including growth, differentiation, apoptosis, and neurotransmission.[12,13] Bryostatin 1 modulates the conventional (cPKC) and novel (nPKC) PKC subtypes by binding to their regulatory C1 domains (C1a and C1b).[14,15] This interaction mimics the actions of their endogenous activator diacylglycerol (DAG), which is transiently produced in the inner leaflet of the plasma membrane in response to activation of numerous receptors. Upon its generation, DAG inserts into the DAG/phorbol ester-binding cleft of the C1 domains of the c/nPKCs, anchoring them at the plasma membrane and driving the conformational change of the PKCs, leading to their enzymatic activation.[5]

Comparison between C1 domains of PKCs and those of other protein families demonstrated a high degree of homology with proteins of the mammalian unc13 (Munc13) family.[12] This family of proteins consists of four isoforms (Munc13-1, Munc13-2, Munc13-3, and Munc13-4) that act as important scaffolds in vesicular priming and exocytosis.[16−19] Of these

Received: May 14, 2019
Revised: May 31, 2019
Published: June 3, 2019

DOI: 10.1021/acs.biochem.9b00427
Biochemistry 2019, 58, 3016−3030

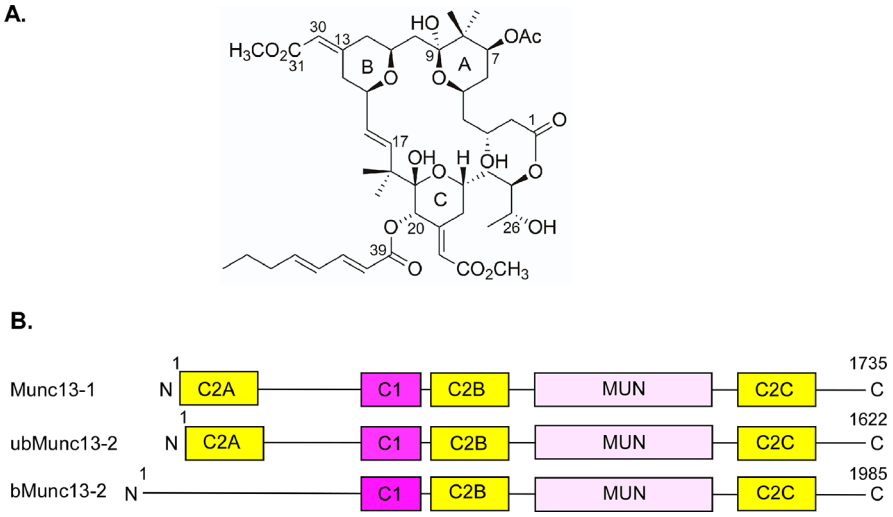

Figure 1. Structures of bryostatin 1 and Munc13s. (A) Chemical structure of bryostatin 1. (B) Domain structure of Munc13-1, ubMunc13-2, and bMunc13-2. The C1 domain binds lipids and DAG/phorbol ester. C2 domains bind lipids and Ca^{2+}. MUN is a self-folding domain consisting of two Munc13 homology domains. Constructs used during experiments contained a green fluorescent protein (GFP) tag at their C-termini.

isoforms, Munc13-1, -2, and -3 are DAG receptors expressed in the brain.[20−23] Among the brain-expressed variants of the Munc13 family, Munc13-1 demonstrates predominate expression in the hippocampal, cerebellar, cortical, and striatal brain regions.[21] Since its discovery, Munc13-1 has been implicated in the maintenance of synaptic plasticity through its modulation of long-term potentiation[24] and has been shown to serve an important role in hippocampal glutamatergic neurotransmission.[25] Today, Munc13-1 is identified as a presynaptic active zone protein that is essential for the priming of synaptic vesicles and neurotransmission.[26−28]

Munc13-1 is critically involved in neurodegenerative disorders and synaptic plasticity.[29−32] For example, Munc13-1 regulates A_β-induced neurotoxicity in an AD model.[30,31,33,34] Clinical studies have reported that single-nucleotide polymorphism in the Munc13-1 gene is associated with amyotrophic lateral sclerosis and frontotemporal dementia.[35−38] Munc13-1 also regulates neuron cell survival at the time of progression of amyotrophic lateral sclerosis.[39] Munc13-1-dependent neurosecretion is essential for immune response and motor neuron degeneration.[40]

Structurally, Munc13-1 consists of five domains that include three C2 domains, a DAG-binding C1 domain, and a MUN domain (Figure 1B).[41,42] For Munc13-1 to carry out its essential function in neuronal transmission, the overall structure of the C1, C2B, and MUN domains is required.[28,41,42] Munc13-2 exists as two splice variants, with the ubiquitously expressed ubMunc13-2 closely resembling the structure of Munc13-1 and the brain specific bMunc13-2 having a distinct N-terminus (missing the first C2 domain).[43]

Bryostatin 1 is a DAG mimetic that effectively modulates the activity of c/nPKCs through interaction with their C1 domains. On the basis of the primary sequence homology, secondary structural resemblance, and common ligands (DAG and phorbol ester) shared by the C1 domains of c/nPKCs and Munc13-1, bryostatin 1 would be expected to function as a Munc13-1 activator and bind to the Munc13-1 C1 domain.[20,44−46] Previously, we had shown that bryostatin 1 bound to the C1 domain of Unc13, which is the *Caenorhabditis elegans* orthologue of Munc13.[47] However, the phorbol ester binding activity of Unc13 was reported to differ dramatically from that of Munc13.[48] Considering the spatial orientation of the conserved Trp-588 residue at the DAG/phorbol ester-binding site of the Munc13 C1 domain, where the tryptophan inserts into the ligand-binding cleft and would thereby compete with binding by ligands, bryostatin 1 might be expected to have a lower affinity for Munc13-1 than for the PKCs.[46] Here, we characterize bryostatin 1 as a ligand for the Munc13-1 C1 domain in isolation and in the context of the full-length protein. We further characterize its ability to induce membrane translocation in intact cells. We describe that bryostatin 1 acts in a similar way on several of the other Munc13 isoforms. Finally, we report that, similar to its effects on c/nPKCs, bryostatin 1 induces changes in the protein expression of the Munc13-1 isoform *in vitro* and *ex vivo*.

MATERIALS AND METHODS

Materials. The phorbol 12-myristate 13-acetate (PMA) was purchased from Sigma-Aldrich (St. Louis, MO) or from LC Laboratories (Woburn, MA). Bryostatin 1 was purchased from Sigma-Aldrich or provided by the Developmental Therapeutics Program of the National Cancer Institute. PDBu was from LC Laboratories. [^{3}H]PDBu (17.2 Ci/mmol) was from PerkinElmer Life Sciences and was a custom radiosynthesis. Immortalized mouse hippocampal cell line HT22 was obtained from ATCC (Manassas, VA). Fetal bovine serum (FBS) was purchased from ZenBio (Research Triangle Park, NC) or from ATCC (in the case of the live cell confocal experiments). *Rattus norvegicus* Munc13 green fluorescent protein constructs were a generous gift from N. Brose (Max Planck Institute for Experimental Medicine, Gottingen, Germany). Munc13-1 antibodies were purchased from Synaptic Systems (Goettingen, Germany). All other reagents were obtained from Thermo Fisher Scientific (Grand Island, NY).

Cell Culture and Transfection for Western Blotting and Confocal Analysis of Fixed Cells. Hippocampus-derived HT22 cells were used for membrane translocation and expression studies. The proliferative HT22 cells were maintained in Dulbecco's modified Eagle's medium (DMEM) supplied with 10% FBS, 2 mM glutamine, penicillin

DOI: 10.1021/acs.biochem.9b00427
Biochemistry 2019, 58, 3016−3030

(100 units/mL), and streptomycin (100 μg/mL) in a humidified atmosphere of 5% CO_2 at 37 °C.

Transfection was performed using Lipofectamine 3000 LTX with Plus reagent following the manufacturer's recommendations.

Twenty-four hours prior to transfection, proliferative HT22 cells were seeded into 12-well plates (6×10^4 cells per well) containing 12 mm glass coverslips (VWE, Atlanta, GA). Once they were 70−80% confluent, cells were transfected with either Munc13-1-GFP, GFP-tagged Munc13-1^{H567K}, or GFP-tagged Munc13-1^{W588A} plasmids using Lipofectamine 3000 LTX with Plus reagent. The optimum reagent ratio consisted of 1 μg of DNA, 1 μL of LTX, and 1 μL of P3000. During transfection, growth medium was replaced with medium deficient in penicillin and streptomycin.

Confocal Microscopy on Fixed Cells. HT22 cells were grown, transfected, and treated with PMA or bryostatin 1 (0.1−2 μM) on coverslips. Cells were washed and fixed with 4% paraformaldehyde (PFA) for 10 min. Coverslips containing cells were mounted to slides using mounting media. Cell fluorescence (Munc13-GFP) was examined, and images were acquired using a confocal microscope (63×, Leica SP8, Leica Microsystems). The subcellular distribution of Munc13 was quantified from confocal images using ImageJ (http://rsb.info.nih.gov/ij/). The mean membrane (membrane size was defined as 300 nm from the outer edge) and whole cell intensities of individual images were measured. The ratios between the mean fluorescence intensity of the membrane and whole cells are presented as described previously.[49,50]

Confocal Microscopy of Living Cells and Quantification of Images. HT22 cells (EMD Millipore) (between passages 2 and 16) were plated on Ibidi dishes (Ibidi, LLC) in high-glucose DMEM containing FBS (10%) and L-glutamine (2 mM) and grown to 80% confluency at 37 °C. After 24 h in culture, cells were transfected with GFP-tagged recombinant constructs, using X-tremeGENE HP DNA transfection reagent (Sigma) according to the manufacturer's recommendations. Twenty-four hours after transfection, cells were transferred to confocal medium (DMEM without phenol red with 1% FBS) and translocation in response to the indicated PMA, bryostatin 1, and PDBu treatments was visualized using a Zeiss LSM 780 NLO or Zeiss LSM 710 NLO confocal microscope (Carl Zeiss, Inc.) equipped with a 63× 1.4 NA oil objective. GFP was excited with an argon laser at 488 nm, and filters of 500−530 nm were used for detecting emission. PMA (1 μM), bryostatin 1 (10, 100, or 1000 nM), and PDBu (1 μM) were added at time zero, and translocation was monitored every 30 s. For quantitation of GFP translocation to the membrane or from the nucleus, two regions of ∼4 μm^2 were selected in each cell over the plasma membrane, nucleus, and cytoplasmic regions at each time point (as indicated in the figures). Mean intensities of the GFP-tagged constructs in the selected regions were calculated using the Zeiss Zen software for the images at the different time points; the ratios of the intensities for the membrane to the cytoplasm or the cytoplasm to the nucleus were then calculated and normalized to the time zero values. The increase in the membrane/cytoplasm or cytoplasm/nucleus ratio indicates translocation. Any cells in which the signal density reflected signal saturation were excluded from the analysis. Imaging was conducted in the Center for Cancer Research Confocal Microscopy Core facility of the National Cancer Institute.

Cell Fractionation and Western Blot Analysis of HT22 Cells Expressing Full-Length Munc Protein Isoforms. Proliferative HT22 cells expressing GFP-tagged Munc13-1 or bMunc13-2 were treated with PMA and bryostatin 1 (1 μM). Subcellular fractionation was performed using the subcellular fractionation kit (catalog no. 78840, Thermo Scientific Inc., Rockford, IL) as per the manufacturer's instructions. The kit efficiently isolates cytoplasmic and membrane fractions for localization and distribution studies. Briefly, treated cells were harvested in ice-cold PBS and lysed in cytosolic extraction buffer (CEB) and then centrifuged at 500*g* for 5 min. The supernatant was the cytosolic fraction. The pellet was dissolved in the membrane extraction buffer and incubated at 4 °C for 10 min. The sample was centrifuged at 3000*g* for 5 min, and the supernatant (membrane extract) was transferred to a chilled tube. The protein concentration of each isolated fraction was measured using the BCA protein estimation kit (Thermo Scientific Inc.), and 40 μg of protein was subjected to sodium dodecyl sulfate−polyacrylamide gel electrophoresis (SDS−PAGE) (4−15% TGX Gel, Bio-Rad, Hercules, CA) and Western blot analysis. Membrane fraction samples were prepared by mixing with loading buffer sample (LSB) and without heating. Antibody dilutions were as follows: 1:500 anti-mouse GFP, 1:500 anti-rabbit GFP, 1:2000 anti-rabbit Na,K-ATPase, and 1:2000 anti-mouse β-actin (Cell Signaling, Danvers, MA). The protein bands were visualized using the Li-COR Odyssey Infrared Imaging System (Li-Cor Biosciences, Lincoln, NE) using goat anti-rabbit IRDye-800CW and goat anti-mouse IRDye-680RD secondary antibodies. The bands were detected and captured in the linear intensity range. The bands were quantitated using ImageJ (http://rsb.info.nih.gov/ij/).

Expression of Endogenous Munc13-1 in HT22 Cells Detected by Immunoblotting. For induction of differentiation, proliferative HT22 cells were incubated in Neuro-Basal medium containing a nitrogen supplement, cAMP, L-glutamine, penicillin, and streptomycin. Approximately 48−72 h after "day 0" of differentiation, cells were treated with different doses of bryostatin 1 (either 0.1 or 0.5 μM). For Western blot analysis, differentiated HT22 cell and primary hippocampal neurons (see below) were collected and resuspended in modified radioimmunoprecipitation assay buffer containing a protease and phosphatase inhibitor mixture. Cell suspensions were sonicated, resuspended, and centrifuged at 14000*g* for 30 min at 4 °C. Lysates were separated via 7.5−10% SDS−PAGE. After the separation, proteins were transferred to nitrocellulose membranes, and nonspecific binding sites were blocked by treatment with 2.5% bovine serum albumin (BSA) in TBS-T. Anti-Munc13-1 (1:500, rabbit polyclonal, Synaptic Systems) and anti-β-actin (1:5000, rabbit polyclonal, Cell Signaling) primary antibodies were used to blot the membranes, followed by incubation with the anti-rabbit HRP (1:5000) secondary antibody. The immunoreactive bands were visualized using ECL reagent (Pierce), and images were captured with an image processer (Alpha Imager Gel Documentation system, Alpha Innotec, Santa Clara, CA). The bands were quantitated using ImageJ (http://rsb.info.nih.gov/ij/).

Primary Neuron Culture. Primary hippocampal neuronal cultures were prepared from the hippocampal tissues of gestational 18-day-old mouse embryos. Experiments were carried out with approval of the Animal Care and Use Committee of the University of Houston. Briefly, hippocampal

DOI: 10.1021/acs.biochem.9b00427
Biochemistry 2019, 58, 3016−3030

tissues were dissected and maintained in ice-cold calcium-free Hank's balanced salt solution (HBSS) and then dissociated in HBSS containing trypsin and 0.25% EDTA for 20 min at 37 °C. The dissociated cells were then plated at an equal density of 8×10^4 cells per well on 12 mm coverslips precoated with 50 μg/mL poly-D-lysine. Cultures were maintained in neuronal feeding medium fortified with B-27 supplement, 200 mM L-glutamine, 100 IU/mL penicillin, 100 μg/mL streptomycin, and HEPES. The cells were maintained in a humidified CO_2 incubator (5% CO_2 and 37 °C) for 24 h. Half of the culture medium was replaced every 3 days. Approximately 7−8-day-old cultures were used for experiments. Primary hippocampal neurons were treated with two different doses of bryostatin 1 (either 0.1 or 0.5 μM). Twenty-four hours post-treatment cells were collected and processed for immunocytochemistry.

Immunocytochemistry for Visualization of Endogenous Munc13-1 in HT22 Cells and Primary Hippocampal Neurons. Differentiated HT22 cells and the primary hippocampal neurons were fixed with 4% PFA in PBS for 15 min and processed for immunocytochemical staining. First, nonspecific sites were blocked with 0.4% BSA, 0.2% Triton X-100, and 0.02% Tween 20 in PBS for 1 h at room temperature. Cells were then incubated overnight at 4 °C with different primary antibodies such as Munc13-1 (1:500, rabbit polyclonal, Synaptic Systems), VGLUT1 (1:500, knockout verified guinea pig polyclonal, Synaptic Systems), and Tuj1 (1:1000, mouse monoclonal, R&D). Appropriate secondary antibodies (ThermoFisher Scientific Inc.) were used followed by incubation with DAPI (Sigma, St. Louis, MO) for 5 min at room temperature to stain the nucleus. Coverslips containing immunostained cells were washed twice with PBS and mounted on slides. Images of cells were captured with a Leica SP8 confocal microscope. The VGLUT1 antibody from Synaptic Systems (catalog 135 304) has been knockout verified and has been extensively used for immunostaining and immunoblotting in >50 articles (https://www.sysy.com/products/vglut1/index.php).

Quantification of Munc13-1 Expression. Quantification of Munc13-1 in the cytosol of differentiated HT22 cells and primary hippocampal neurons was performed as follows. In each independent experiment, a total of three wells of cultured primary hippocampal neurons or differentiated HT22 cells per experimental group were immunostained with antibodies directed against Munc13-1 as described above. After immunofluorescent staining, three individual cells were imaged from each well using 63× (3.5× zoom) magnification. The mean intensity of the fluorescence of Munc13-1 in the cytosol was measured using LAS X software (Leica Microsystem Inc.). Data were expressed as the mean intensity of Munc13-1 in the cytosol.

***In Vitro* [^{3}H]PDBu Binding Assays.** The phorbol ester binding affinities of the Munc13-1 full-length protein and the C1 domain of Munc13 [wild type (WT) or W22A mutant] were determined by the *in vitro* [^{3}H]PDBu binding assay developed in the Blumberg laboratory and described in detail previously.[51] All measurements were taken at 37 °C for 5 min in the presence of 100 μg/mL lipid of the indicated compositions (phosphatidylserine:phosphatidylcholine, w:w) and 0.1 mM Ca^{2+} to obtain the individual inhibition constants (K_i values). The binding of full-length protein and the W22A mutant C1 domain was measured in 100% PS in the presence of 25 and 500 nM [^{3}H]PDBu, respectively, while that of the WT C1 domain was measured in 5:95 PS/PC, 20:80 PS/PC, and 100:0 PS/PC mixtures in the presence of 100 nM [^{3}H]PDBu. The K_d values for the proteins were determined earlier under the same conditions.[52] K_i values in competition experiments were calculated from the measured IC_{50} values as described by Cheng-Prusoff,[53] which corrects for the rightward shift of competition curves dependent on the concentration of the radioligand relative to the K_d of the radioligand. Nonspecific binding was measured as described previously[51] in the presence of 40 μM nonradioactive PDBu. All competition experiments were performed at least three times. In each experiment, each point in the competition curve represents triplicate determinations, and each curve is determined from at least six concentrations of a competitor together with a control without a competitor.

Expression and Purification of GST-Tagged Munc13-1 C1 Domains from *Escherichia coli* for Analysis of Ligand Binding. The WT Munc13-1 C1 domain and W22A mutant used for analysis of ligand binding were expressed and purified as described previously.[52]

Expression and Purification of Full-Length Munc13-1. The expression and purification of full-length rat Munc13-1 from transfected HEK-293 cells for analysis of ligand binding were performed as described previously.[52]

Molecular Docking. Bryostatin 1 was docked into the Munc13-1 C1 domain [Protein Data Bank (PDB) entry 1Y8F] using AUTODOCK 4.2.[54] The docking simulations were prepared, run, and analyzed using AutoDockTools (ADT). The crystal structure of bryostatin 1 was obtained from the Cambridge Structural Database.[55] Energy minimization was carried out using the steepest descent method to remove steric clashes in the proteins and bryostatin 1 using the Amber force field parameters in Chimera.[56] Kollman charges and Gasteiger charges were assigned to the proteins and bryostatin 1, respectively. A grid was generated and centered on the geometry of the phorbol ester in phorbol ester-bound PKCδ C1B (PDB entry 1PTR). The grid included the active site between the two loops of the C1 domain within a box size set at x = 40 Å, y = 55 Å, and z = 40 Å. The Lamarckian Genetic Algorithm (LGA) was used to search for the best 20 conformers during the docking simulations. The bryostatin 1-docked structures were visualized using Discovery Studio Visualizer 4.5 (Biovia Inc.).

Statistical Analysis. Data analysis was performed using Prism 7.0 software (GraphPad Software, Inc., San Diego, CA). All statistical analyses were performed on the basis of at least three independent experiments. Raw data from PMA and bryostatin 1 treatments of proliferative HT22 cells were analyzed using two-way analysis of variance. Raw data from bryostatin 1 treatments of differentiated HT22 cells and primary hippocampal neurons were analyzed using one-way analysis of variance (ANOVA). After an initial statistical significance test, Tukey's multiple-comparison post hoc tests were performed to compare all treatment groups. Differences with $P < 0.05$ were considered significant.

RESULTS

Binding of Bryostatin 1 to Full-Length Munc13-1 and Its C1 Domain. We have previously described that PDBu binds to the C1 domain of Munc13-1 but with an affinity that is modestly weaker than that found for the C1B domain of PKCδ or the C1 domain of RasGRP3. Reflecting its unusual overall charge, being negatively charged whereas C1 domains are usually positively charged, the Munc13-1 C1 domain

DOI: 10.1021/acs.biochem.9b00427
Biochemistry 2019, 58, 3016−3030

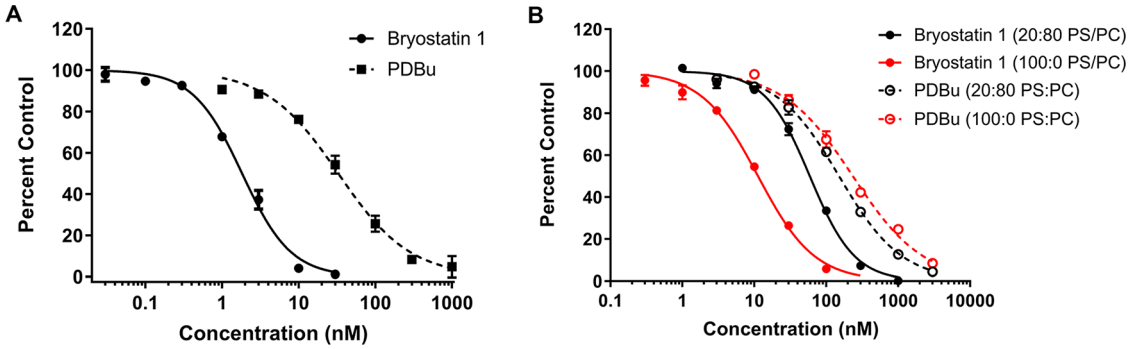

Figure 2. (A) Concentration-dependent displacement of [^{3}H]PDBu from purified full-length Munc13-1 by bryostatin 1 and PDBu. Binding of [^{3}H]PDBu (25 nM) to the purified full-length Munc13-1 was measured in the presence of 100 μg/mL lipid (100% PS), 0.1 mM Ca^{2+}, and different concentrations of bryostatin 1 and PDBu. Data points represent the mean ± the standard error of the mean (SEM) of three experimental values in a single experiment. Where error bars are not visible, they lie within the symbols. Two additional experiments gave similar results. Note that the curves yield IC_{50} values, from which K_i values reported in the text are derived through the Cheng-Prusoff relationship.[53] (B) Lipid dependence of binding of bryostatin 1 to the C1 domain of Munc13. Binding of [^{3}H]PDBu (100 nM) to the purified C1 domain of Munc13-1 was measured in the presence of 0.1 mM Ca^{2+}, 100 μg/mL lipid [20:80 PS/PC (black lines) or 100% PS (red lines)], and different concentrations of bryostatin 1 and PDBu. Data points represent means ± SEM of three experimental values in a single experiment. Where error bars are not visible, they lie within the symbols. Two additional experiments gave similar results. Note that the curves yield IC_{50} values, from which the K_i values reported in the text are derived through the Cheng-Prusoff relationship.[53]

Table 1. Binding of Bryostatin 1 and PDBu by the Munc13-1 C1 Domain and Its Mutant[a]

	K_i for bryostatin 1 (nM)			K_d for PDBu (nM)		
lipid conditions	5:95 PS/PC	20:80 PS/PC	100:0 PS/PC	5:95 PS/PC	20:80 PS/PC	100:0 PS/PC
Munc13-1 FL			0.45 ± 0.04			7.09 ± 0.53
Munc 13-1 C1 WT	22.8 ± 1.8[b]	22.68 ± 0.54[b]	8.07 ± 0.90	82 ± 15	69.5 ± 4.8[c]	124 ± 13
Munc 13-1 C1 W22A mutant			54 ± 12			808.6 ± 8.1

[a]The bryostatin 1 binding affinity (K_i) and the PDBu binding affinity (K_d) were determined for the full-length (FL) Munc13-1 and the C1 domain of Munc13-1 wild type (WT) and its mutant under three different lipid conditions. Values represent the mean ± SEM from three independent experiments. One-way ANOVA, followed by Tukey's post hoc test, was used for the analysis of statistical significance. [b]$P < 0.001$ compared to 100% PS in K_i for bryostatin 1. [c]$P < 0.05$ compared to 100% PS in K_d for PDBu.

showed an unusual preference for a phospholipid environment with reduced phosphatidylserine. Additionally, the full-length Munc13-1 protein showed enhanced affinity compared to that of the isolated C1 domain, presumably reflecting the influence of the C2B domain in promoting its membrane interaction.[52]

Bryostatin 1 bound with an affinity higher than that of PDBu to the isolated C1 domain of Munc13-1. Assayed in the presence of a PS/PC (20:80, w:w) mixture, its K_i was 22.7 ± 0.5, compared to a value of 69.5 ± 4.8 nM for PDBu, assayed in parallel (Figure S1). (Note that Figure S1 shows the measured IC_{50} values; K_i values are calculated from the IC_{50} values, as described by Cheng-Prusoff,[53] to correct for the rightward shift in the IC_{50} caused by competition with the fixed concentration of radioligand present.) As seen for PDBu, the full-length Munc13-1 protein also bound bryostatin 1 with an affinity higher than that of the isolated C1 domain. Bryostatin 1 bound to the full-length Munc13-1 protein with a K_i of 0.45 ± 0.04 nM. It thus had an affinity approximately 15-fold better than that of PDBu (K_i = 7.1 ± 0.5 nM) measured in parallel, where these measurements were carried out in 100% PS (Figure 2A and Table 1; note that figure shows IC_{50} values, from which K_i values are calculated as described by Cheng-Prusoff[53]).

The optimal conditions for binding of bryostatin 1 to the isolated Munc13-1 C1 domain were different from those for PDBu in that bryostatin 1 preferred a lipid environment with a higher proportion of PS. Comparison of assays in the PS/PC (20:80) and PS/PC (100:0) lipid mixtures showed that the K_i for bryostatin 1 improved from 22.7 + 0.5 to 8.0 + 0.9 nM in the PS/PC (100:0) mixture, whereas the K_i for PDBu became modestly poorer, changing from 69.5 ± 4.8 to 124 ± 13 nM. Thus, depending on the lipid environment, bryostatin 1 displayed an affinity better than that of PDBu between 3-fold at lower PS concentrations and 15-fold in 100% PS (Figure 2B and Table 1).

We had described previously that the W588A mutation in the C1 domain of Munc13-1 (W22A in the isolated C1 domain) conferred weaker PDBu binding affinity.[52] The binding of bryostatin 1 to the W588A mutant of the isolated C1 domain showed a decrease in affinity similar to that observed for PDBu (6.6-fold for bryostatin 1 vs 6.5-fold for PDBu) (Figure S1 and Table 1).

Bryostatin 1 Induces the Plasma Membrane Translocation of Munc13-1. The assays described above were carried out *in vitro* using purified proteins. To test the actions of bryostatin 1 on Munc13-1 in the context of the physiological environment, we expressed the full-length Munc13-1-GFP construct in the HT22 cells and challenged with bryostatin 1 and PMA. Cells were imaged by confocal microscopy 5 min after treatment (Figure 3).

Both ligands induced translocation of Munc13-1 to the plasma membrane with similar potencies and extents of translocation. Likewise, cell fractionation and immunoblot analysis indicated that, after treatment of HT22 cells for 5 min with bryostatin 1 and PMA (1 μM), both ligands caused Munc13-1 to transfer to the membrane fraction (Figure 4).

DOI: 10.1021/acs.biochem.9b00427
Biochemistry 2019, 58, 3016−3030

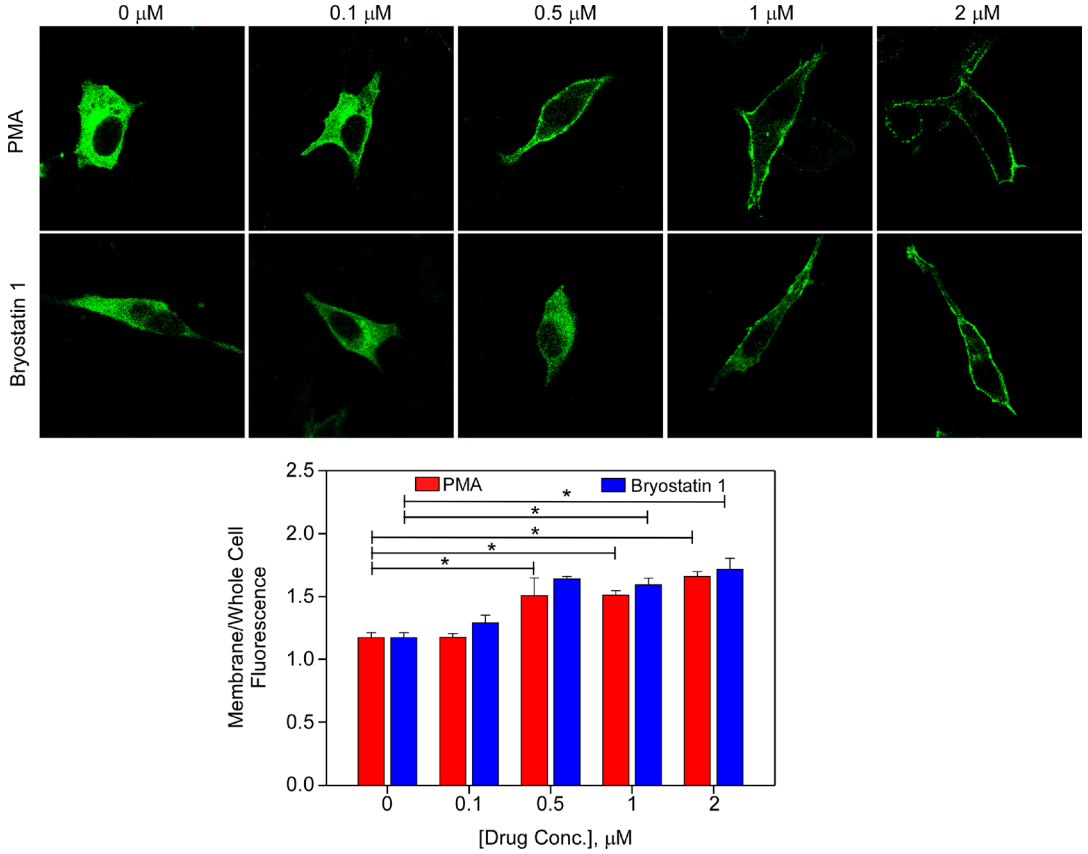

Figure 3. Effect of PMA and bryostatin 1 on Munc13-1 membrane translocation. The top panel shows representative confocal images showing HT22 cells expressing Munc13-1, treated with PMA or bryostatin 1 (0−2 μM) for 5 min. The bottom panel shows a bar graph of values for the normalized membrane to whole cell fluorescence intensity ratio, quantified from confocal images from the multiple experiments, of which the top panel is representative. Data are expressed as means ± SEM of at least three independent experiments and obtained from four to nine confocal cell images per treatment. Two-way ANOVA, followed by Tukey's post hoc test, was used for analysis of statistical significance. *$P < 0.05$ compared to the vehicle control. HT22 cells were transiently transfected with Munc13-1, and confocal image analysis was carried out as described in Materials and Methods.

These results indicate that bryostatin 1 can successfully recruit Munc13-1 from the cytosol to the plasma membrane.

The Translocation of Munc13-1 in Response to Bryostatin 1 Occurs by Binding to Its C1 Domain. To exclude the possibility that the translocation of Munc13-1 in response to bryostatin 1 treatment of HT22 cells was simply due to some indirect effect, such as phosphorylation of Munc13-1 after activation of endogenous protein kinase C by the bryostatin 1, we examined the dependence of the translocation on the Munc13-1 C1 domain. As described by Betz et al.,[20] a His to Lys point mutation at position 567 in the Munc13-1 C1 domain distorts the loops forming the DAG/phorbol ester-binding pocket and renders Munc13-1 unresponsive to the actions of DAG and phorbol ester.

We therefore expressed the GFP-tagged Munc13-1^{H567K} in HT22 cells, challenged with PMA and with bryostatin 1, and assessed the response by confocal microscopy (Figure 5). Mutant Munc13-1^{H567K} showed no significant changes in localization upon treatment. We conclude that, as expected, the translocation of Munc13-1 by bryostatin 1 involves a direct effect of bryostatin 1. It is important to emphasize, however, that this experiment cannot exclude the possibility that Munc13-1 translocation also requires indirect effects of the treatment, such as through activation of PKC. Mutation of Trp-588 to Ala in the C1 domain of Munc13-1 decreased but did not abolish its *in vitro* binding to phorbol ester[52] or to bryostatin 1 (Table 1). After expression of full-length GFP-tagged Munc13-1^{W588A} in HT22 cells, translocation was lost in response to bryostatin 1 but not to PMA, both at 1 μM (Figure 6). This suggests that bryostatin 1 and PMA show a somewhat different dependence on Trp-588 for membrane translocation of full-length Munc13-1. We conclude that, as expected, the translocation of Munc13-1 by bryostatin 1 involves a direct effect of bryostatin 1 on the C1 domain.

Full-Length Munc13-1 and Its Isolated C1 Domain Translocate to Different Intracellular Locations. The translocation studies described above were all carried out on the full-length Munc13-1 protein. Given the differences in the *in vitro* binding affinities and lipid dependence of the isolated Munc13-1 C1 domain and the full-length protein, we wished to compare in parallel their behavior in living cells. Expressed in HT22 mouse hippocampal neuronal cells, the GFP-tagged C1 domain localized to the nucleus and the cytoplasm (Figure 7A) while the full-length protein was solely localized to the cytoplasm in the cells (Figure 7B). After addition of 1 μM bryostatin 1, the GFP-C1 domain (Figure 7A) translocated within 5−20 min from the nucleus to internal membranes but not to the plasma membrane. In contrast, full-length Munc13-1 (Figure 7B) translocated to the plasma membrane. A similar pattern of translocation for the Munc13-1 C1 domain and the full-length protein was seen upon treatment with 1 μM PMA and PDBu. We have previously reported that in LNCaP cells,

DOI: 10.1021/acs.biochem.9b00427
Biochemistry 2019, 58, 3016−3030

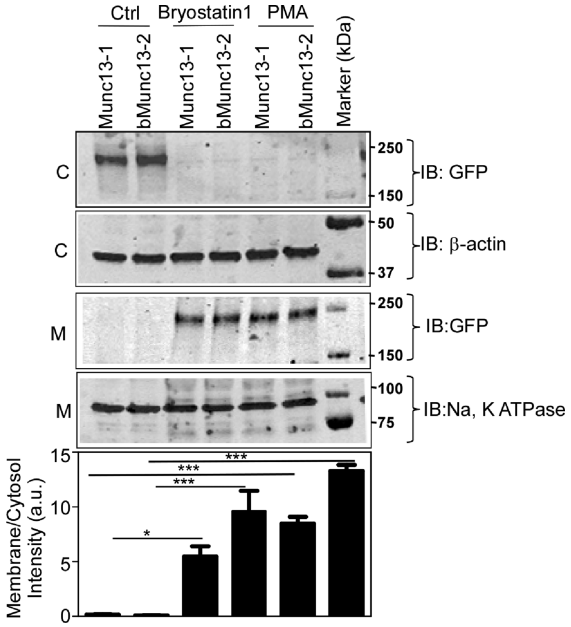

Figure 4. Effect of PMA and bryostatin 1 on Munc13-1 and bMunc13-2 membrane translocation. The top panel shows representative Western blot analysis of the cytosolic (C) and membrane (M) fractions of Munc13-1 and bMunc13-2 after cells were treated with PMA or bryostatin 1 (1 μM) for 5 min. The bottom panel bar graph shows normalized densitometric analysis of immunoblots from multiple experiments, of which the top panel is representative. Data are expressed as means ± SEM of four independent experiments. One-way ANOVA, followed by Tukey's post hoc test, was used for analysis of statistical significance. *$P < 0.05$ compared to the vehicle control for Munc13-1 and bMunc13-2. **$P < 0.01$ compared to the vehicle control for Munc13-1 and bMunc13-2. HT22 cells were transiently transfected with Munc13-1 and bMunc13-2, and Western blot analysis was carried out as described in Materials and Methods.

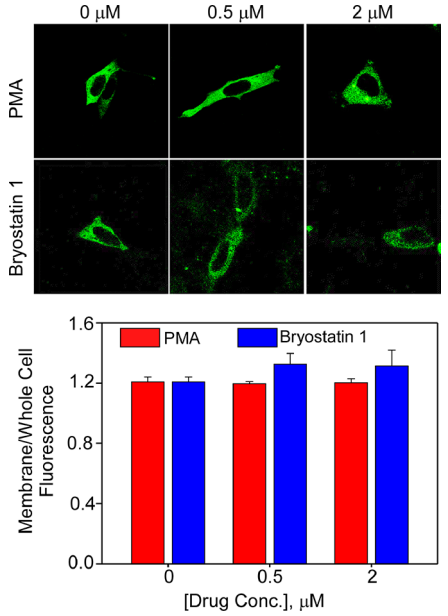

Figure 5. Effect of PMA and bryostatin 1 on Mun13-1^{H567K} membrane translocation. The top panel shows representative confocal images showing HT22 cells expressing Mun13-1^{H567K}, treated with PMA or bryostatin 1 (0−2 μM) for 5 min. The bottom panel bar graph shows values of the normalized membrane to the whole cell fluorescence intensity ratio, quantified from confocal images from the multiple experiments, of which the top panel is representative. Data are expressed as means ± SEM of at least three independent experiments and obtained from three to six confocal cell images per treatment. Two-way ANOVA, followed by a Tukey's post hoc test, was used for analysis of statistical significance. No statistically significant differences were observed. HT22 cells were transiently transfected with Mun13-1^{H567K}, and confocal image analysis was carried out as described in Materials and Methods.

as observed here for the HT22 cells, full-length Munc13-1 translocates to the plasma membrane while the C1 domain alone does not.[52] Consistent with our *in vitro* binding studies, PDBu was modestly less effective than was bryostatin 1 for inducing translocation.

Comparison of Translocation of Full-Length Munc13-1, ubMunc13-2, and bMunc13-2 in Response to Bryostatin 1. ubMunc13-2 and bMunc13-2 represent splice variants of the gene UNC13B and, like Munc13-1, have been shown to be important for vesicle priming. We therefore examined by confocal microscopy the ability of bryostatin 1 to induce the translocation in HT22 cells of GFP-tagged ubMunc13-2 and bMunc13-2 with varying times and doses (Figure 8A). Both showed clear translocation in response to bryostatin 1 with a similar time course as observed for Munc13-1, assayed in parallel, and with modestly greater sensitivity, as reflected by the extents of the response at 100 and 10 nM bryostatin 1. In the same experiments, the time and dose response of GFP-tagged PKCδ was examined (Figure 8B). Bryostatin 1 induces translocation of PKCδ to the nuclear membrane and to internal membranes, rather than to the plasma membrane, but the dose dependence was similar to that for Munc13.

When tested by immunoblotting and confocal microscopy, GFP-tagged bMunc13-2 showed a translocation similar to that of GFP-tagged Munc13-1 in HT22 cells treated with PMA or bryostatin 1 (Figure 4 and Figures S2 and S3).

These results provide strong support for the potential role of Munc13 in the actions of bryostatin 1.

Molecular Docking Simulation. To understand the binding modes of bryostatin 1 in Munc13-1 C1 domain from a structural point of view, we docked bryostatin 1 into the C1 domain (Figure 9A). The structure of the Munc13-1 C1 domain closely resembles that of the PKCδC1B domain.[12] The two loops of the C1 domain form a ligand-binding site in most of the C1 domains. As both bryostatin 1 and phorbol ester act as activators of PKC and Munc13-1, we docked bryostatin 1 into the phorbol ester-binding site of PKC. The predicted bryostatin 1-bound structure with lowest binding energy was selected from the largest cluster generated by an AutoDock Tools script. Our results show that bryostatin 1 interacts mainly with three residues of the Munc13-1 C1 domain (Trp-588, Ile-590, and Arg-592) through hydrophobic interactions and hydrogen bond formation with a binding energy of 1.12 kcal/mol (Figure 9B). Bryostatin 1 forms two hydrogen bonds, one between the C39 carboxyl group of bryostatin 1 and the guanidino group of Arg-592 and one between the C26 hydroxyl group and the backbone carbonyl group of Ile-590.

While our modeling data predict the putative site of bryostatin 1 action in the Munc13-1 C1 domain, it should be noted that the docking simulation was conducted in the absence of any lipid membrane system, which certainly influences the binding affinity. Furthermore, there is a

DOI: 10.1021/acs.biochem.9b00427
Biochemistry 2019, 58, 3016−3030

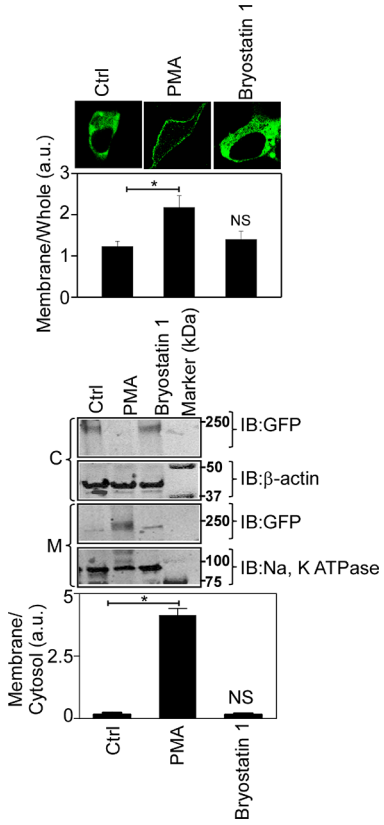

Figure 6. Effect of PMA and bryostatin 1 on Munc13-1^{W588A} membrane translocation. The top panel shows representative confocal images of HT22 cells expressing Munc13-1^{W588A} treated with PMA or bryostatin 1 (1 μM) for 5 min. The bottom panel shows Western blot analysis of the cytosolic (C) and membrane (M) fractions of Munc13-1^{W588A} after cells were treated with PMA or bryostatin 1 (1 μM) for 5 min. The corresponding bar graphs with quantitative analyses for multiple experiments, of which the images are representative, are shown below. Data are expressed as means ± SEM of at least three independent experiments and obtained from three immunoblots or three or four confocal cell images. One-way ANOVA, followed by a Tukey's post hoc test, was used for analysis of statistical significance. *P < 0.001 compared to control (Ctrl). NS, not significant.

possibility that Trp-588, which occludes the phorbol ester/DAG-binding site in Munc13-1, can change its orientation in the native environment as predicted earlier in our molecular dynamics simulation studies.[52]

Bryostatin 1 Upregulates the Expression of Endogenous Munc13-1 in HT22 Cells and Primary Hippocampal Cells. The various targets of phorbol esters such as the PKC isoforms and members of the RasGRP family are involved in complex regulatory feedback loops, where ligand binding and target activation may affect both downregulation and the level of transcription. We find similarly that endogenous Munc13-1 levels are affected by bryostatin 1 treatment. Differentiated HT22 cells were treated with two different doses of bryostatin 1 (either 0.1 or 0.5 μM). Twenty-four hours post-treatment, cells were collected and immunostained for endogenous Munc13-1 expression (Figure 10A). VGLUT1 co-stained with Munc13-1 provides a marker of differentiated HT22 cells. The level of endogenous Munc13-1 staining increased with both doses of bryostatin 1 (0.1 and 0.5 μM) (Figure 10B). Likewise, endogenous Munc13-1 levels were increased by the bryostatin 1 treatment as determined by Western blot analysis (Figure 10C,D). Bryostatin 1 had similar effects in an *ex vivo* system. Mouse primary hippocampal neurons were cultured from 18-day-old prenatal pups and treated with either 0.1 or 0.5 μM bryostatin 1 for 24 h. We observed increased levels of expression of endogenous Munc13-1 in the cytosol of Tuj-1 positive neuronal cells (Figure 11). In addition, quantitation of Munc13-1 expression revealed that both doses of bryostatin 1 significantly increased the level of expression of Munc13-1 in comparison to the control. These results clearly show that bryostatin 1 upregulates the expression of Munc13-1 in neuronal cells. While we did not investigate this upregulation in further detail, such upregulation provides a second mechanism by which bryostatin 1 can influence Munc13-1 activity.

DISCUSSION

Among natural products targeting C1 domains, which represent the recognition motif for the ubiquitous lipid second messenger diacylglycerol, the bryostatins have attracted particular attention because of their unique spectrum of biological effects. Recently, particular interest has been directed at the neuroactive effects of the bryostatins, and this activity has led to their clinical trials for dementia. Mechanistically, protein kinase C ε (PKCε) is thought to be a critical contributor to these neuron effects. However, Munc13-1 is also known to have a DAG/phorbol ester responsive C1 domain and is of great importance for its priming of neuronal vesicle release. The goal of this study was therefore to characterize the interaction of bryostatin 1 with the C1 domain of Munc13-1, to explore how its behavior was modified by the context of the C1 domain in the intact Munc13-1 protein and by the physiological membrane environment, and finally to assess the modulatory actions of bryostatin 1 on Munc13-1 protein expression.

Bryostatin 1 recruits Munc13-1 to the plasma membrane in a fashion largely similar to that of phorbol ester. As with the classic and novel PKCs, bryostatin 1 binds to the C1 domain of Munc13-1 and this binding is essential for the membrane translocation of the protein, although we cannot exclude the possibility that other targets of bryostatin 1 make a further, indirect contribution to the translocation. The position of Trp-588 in the C1 domain of Munc13-1 is similar to that which it occupies in many of the C1 domains of the PKCs, and this Trp residue has been shown to be an important contributor to membrane association and potent ligand binding.[52] Somewhat unexpectedly, mutation of Trp-588 to alanine blocked the translocation of Munc13-1 in response to bryostatin 1 but not PMA, both at 1 μM. Most probably, the difference reflects the fact that PMA, being more hydrophobic than bryostatin 1, is better able to compensate for the reduced hydrophobicity of the C1 domain with the W588A mutation. An unusual feature of the Munc13-1 C1 domain is that it is negatively charged, whereas the C1 domains of almost all of the other DAG/phorbol ester-binding C1 domains are positively charged. Consistent with the charge conflict between the Munc13-1 C1 domain and the membranes, the Munc13-1 C1 domain preferred a lower phosphatidylserine content in the membrane than was typical. Similarly, the full-length Munc13-1 protein, which has other membrane-binding elements, bound bryostatin 1 with an affinity higher than that of the isolated C1 domain, consistent with these other elements assisting in the membrane association of the ternary C1 domain−bryostatin 1 complex. Finally, bryostatin 1 treatment induced the

DOI: 10.1021/acs.biochem.9b00427
Biochemistry 2019, 58, 3016−3030

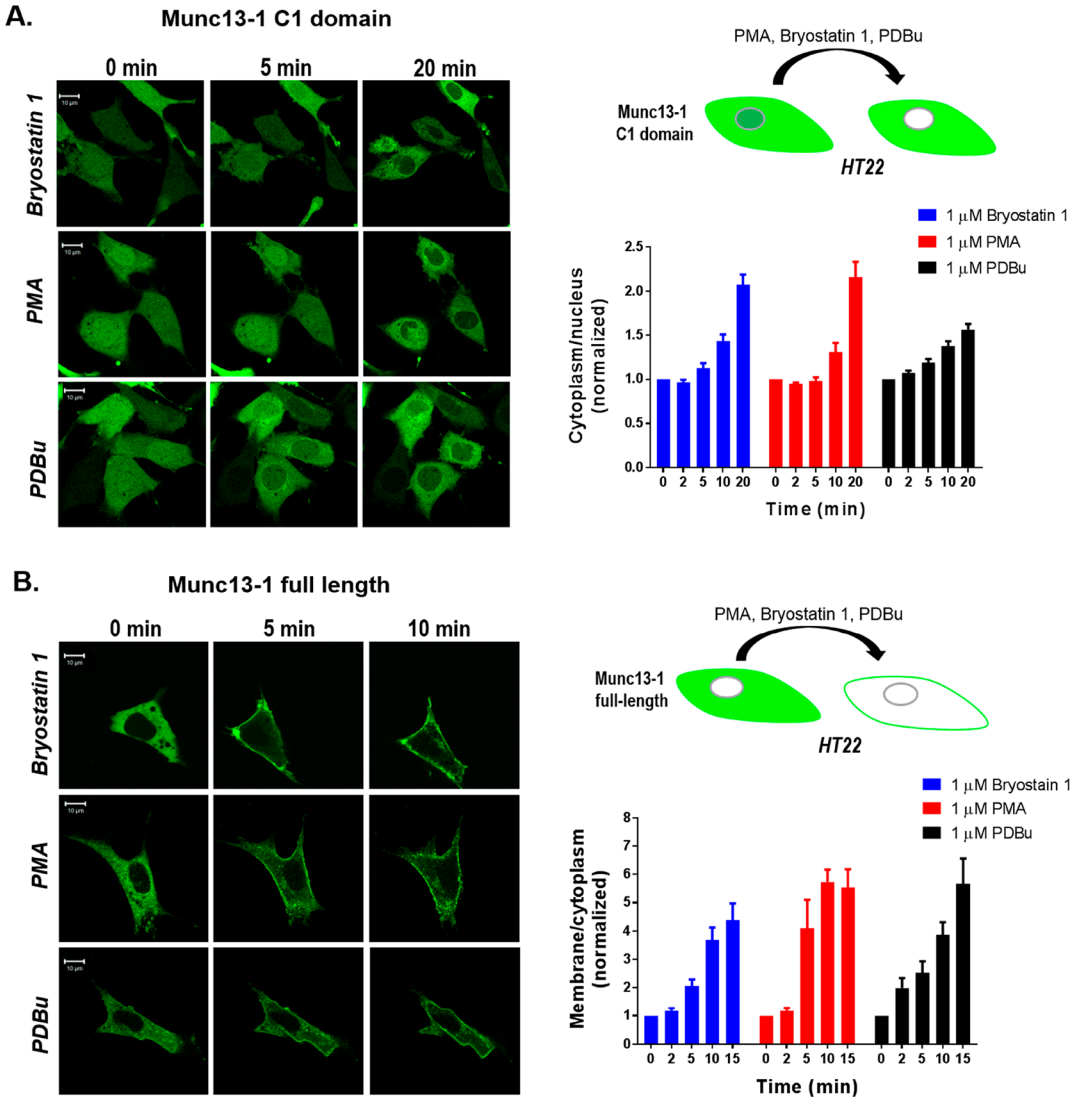

Figure 7. Translocation in response to PMA, bryostatin 1, and PDBu of (A) the GFP-tagged Munc13-1 C1 domain and (B) the full-length Munc13-1 protein in living HT22 cells. Cells expressing the GFP-tagged Munc13-1 C1 domain and the full-length Munc13-1 were treated with 1 μM bryostatin 1, PMA, and PDBu. The living cells were imaged by confocal microscopy as a function of time after addition of bryostatin 1, PMA, and PDBu. The images are representative of three independent experiments, and the ratios of the intensities for the cytoplasm to the nucleus (Munc13-1 C1 domain, 11−16 cells/treatment, A) or the membrane to the cytoplasm (Munc13-1 full-length, 5−9 cells/treatment, B) were calculated and normalized to the time zero values. An increase in the cytoplasm/nucleus or membrane/cytoplasm ratio indicates translocation. Values represent the mean of the three independent experiments. Bars indicate the SEM.

upregulation of endogenous Munc13-1 in both hippocampus-derived cells and hippocampal primary neurons, representing a second mechanism whereby it could positively influence Munc13-1 activity.

Particular attention has been directed at the role of PKCε in the neuroprotective role of bryostatin 1. Our results indicate that Munc13-1 is also a potentially relevant target for neuronal actions of bryostatin 1. Early results of the analysis of the C1 domain of Munc13 had suggested that it possessed a weaker affinity for the phorbol esters than was typical for the C1 domains of the PKCs, or at least the higher-affinity C1 domain of the tandem C1 domains in the various PKC isoforms, a result that we showed also applied to bryostatin 1. On the other hand, strong binding affinity was restored in the full-length protein. The crystal structure of Munc13-1 provides possible insight into the basis for this improved affinity. The C2B domain, which lies adjacent to the C1 domain, forms charge pairs with several of the negative charges on the C1 domain, helps to orient the C1 domain, and contributes to membrane binding.[28] Additionally, there is no indication that the C1 domain-binding cleft is occluded by other residues in the protein. This contrasts with the findings for PKCβII,[57] RasGRP1,[58] and β2-chimaerin,[59] where residues from other domains in the full-length protein occlude the binding site, requiring that these interactions be broken for the C1 domain to bind the ligand.

The finding that full-length Munc13-1 bound bryostatin 1 with an affinity (K_i) of 0.45 ± 0.04 nM *in vitro* argues that Munc13-1 is a potential relevant target for bryostatin 1 in a therapeutic setting. This value falls well in the range (1.2−5.6 nM) reported previously for the PKC isoforms, assayed under somewhat different conditions.[60] A similar conclusion holds when the translocation of Munc13-1 in response to bryostatin 1 was compared with that of PKCδ. While translocation is

DOI: 10.1021/acs.biochem.9b00427
Biochemistry 2019, 58, 3016−3030

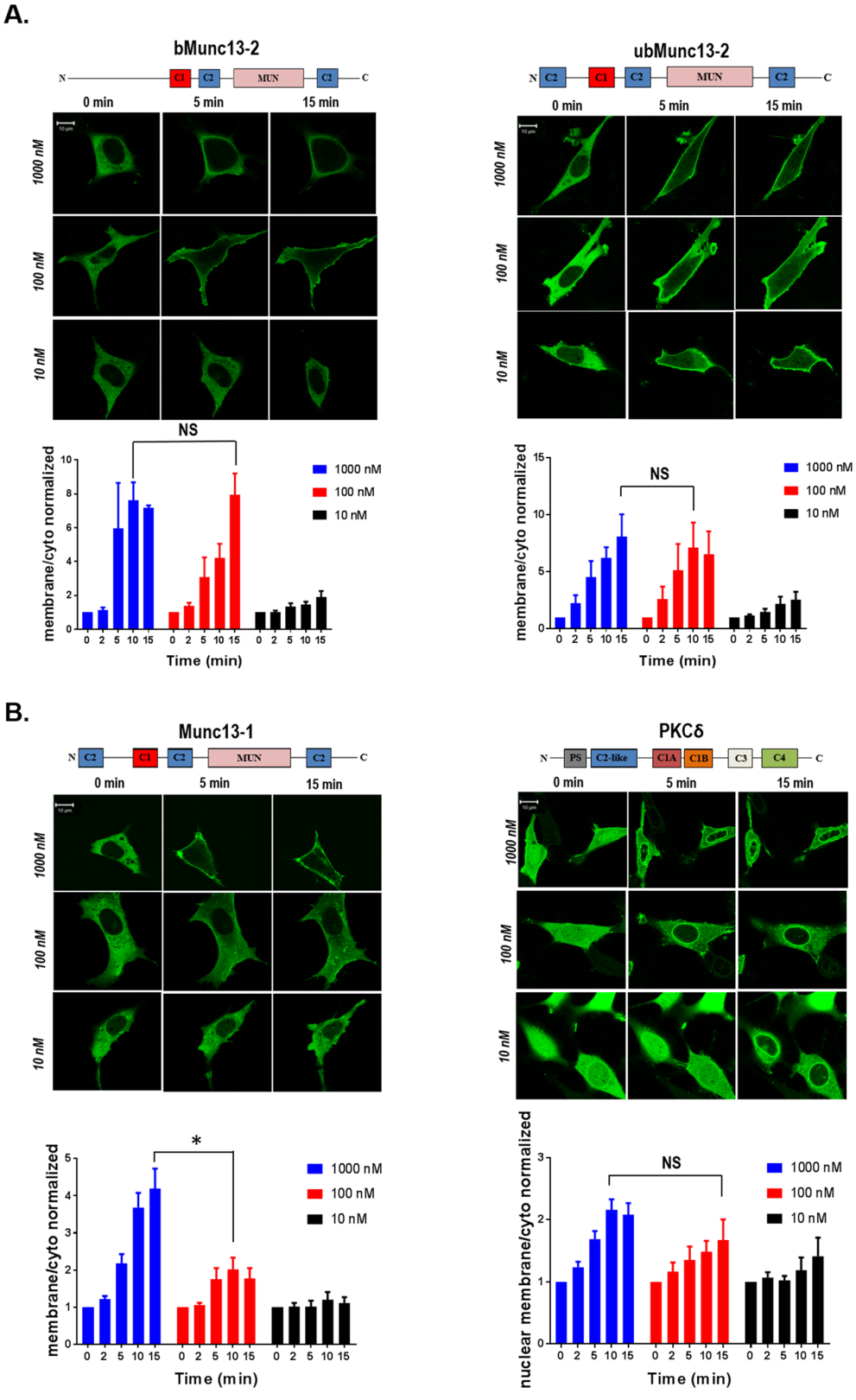

Figure 8. Translocation as a function of time and concentration of bryostatin 1 for the (A) GFP-tagged bMunc13-2 and ubMunc13-2 and (B) Munc13-1 and PKCδ in living HT22 cells. Cells expressing the GFP-tagged Munc13-1, Munc13-2 variants, and PKCδ were treated with 1 μM, 100 nM, and 10 nM bryostatin 1. The living cells were imaged by confocal microscopy as a function of time after addition of the different doses of bryostatin 1. The images are representative of three independent experiments, and the ratios of the intensities for the plasma membrane to the cytoplasm (Munc13-1, 5−9 cells per bryostatin 1 concentration; bMunc13-2, 3−6 cells per bryostatin 1 concentration; and ubMunc13-2, 5−9 cells per bryostatin 1 concentration) or the nuclear membrane to the cytoplasm (PKCδ, 4−7 cells per bryostatin 1 concentration) were calculated and normalized to the time zero values. The increase in the membrane/cytoplasm ratio indicates translocation. Values are presented for time points at 0, 2, 5, 10, and 15 min. Values represent the mean of the three independent experiments. Bars indicate the SEM. The increased level of

DOI: 10.1021/acs.biochem.9b00427
Biochemistry 2019, 58, 3016−3030

Figure 8. continued

translocation of Munc13-1 upon treatment with 1000 nM bryostatin 1 as compared to that with 100 nM bryostatin 1 was significant at the $P = 0.03$ level; the difference in response between treatment with 1000 M and 100 nM bryostatin 1 in the case of bMunc13-2, ubMunc13-2, and PKCδ was not significant ($P > 0.05$). For Munc13-1, 100 nM bryostatin 1 induces a 30% stimulation of that caused by 1000 nM bryostatin 1 (15 min value), while for PKCδ, this fraction is 63%. NS, not significant.

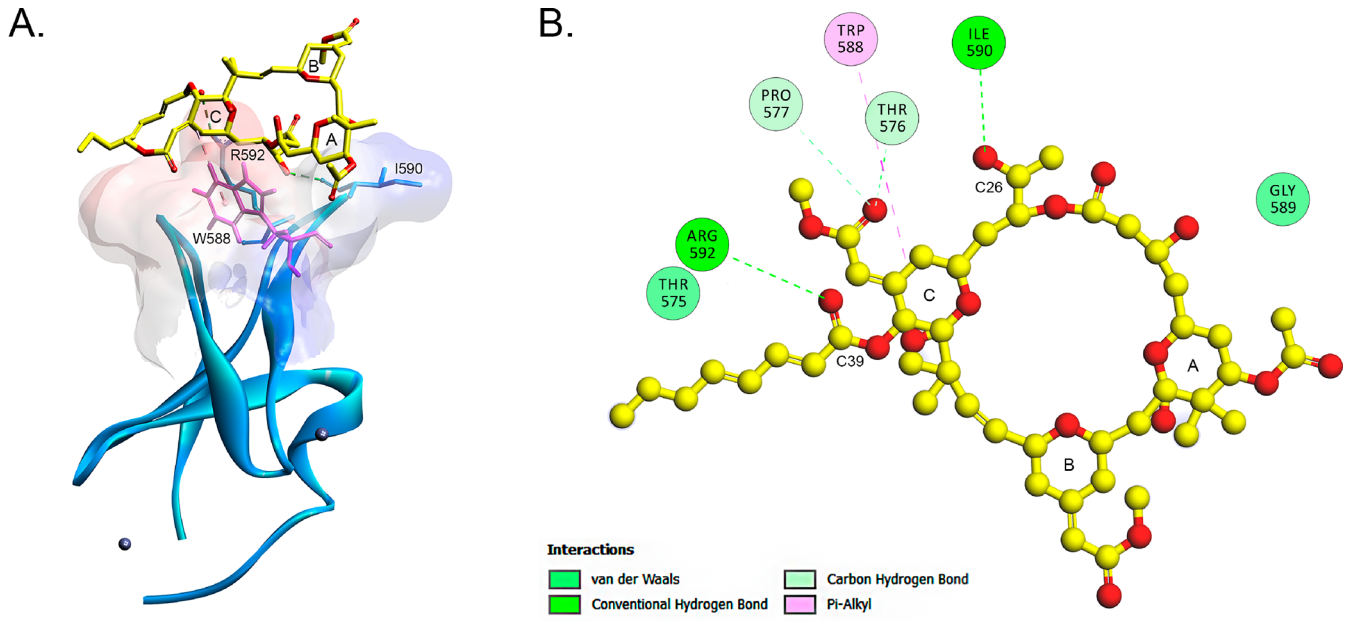

Figure 9. Interaction of bryostatin 1 and Munc13-1. (A) Rim of the active site of the Munc13-1 C1 domain and the docking pose of bryostatin 1 on the Munc13-1 C1 domain. The ribbon structure of the C1 domain of Munc 13-1 with the two Zn ions (balls) is shown. The surface of the structure is colored by hydrophobicity according to the Kyte−Doolittle scale. Blue indicates strong hydrophobicity, and red indicates weak hydrophobicity. The line structure represents bryostatin 1 (yellow). (B) Bryostatin 1 forms two hydrogen bonds (green) and one hydrophobic interaction (magenta) with the residues of the two C1 domain loops.

harder to precisely quantitate than is ligand binding, translocation has an advantage in that it reports the response in the context of physiological rather than artificial membranes. In the HT22 neuronal cells, the Munc13 proteins showed a dose dependence for translocation similar to that of PKCδ.

While the focus on our characterization was on the response of Munc13-1 to bryostatin 1, we also examined the response of the two splice variants of Munc13-2 to bryostatin 1. Together with Munc13-1, Munc13-2 contributes to vesicle priming. We confirmed that the Munc13-2 variants were also responsive to bryostatin 1 and could thus play a role in its neural effects. In addition, the results were suggestive that the two Munc13-2 splice variants might even be a little more responsive than was Munc13-1. If so, it might be possible to build on such a difference for the design of selective second-generation bryostatin analogues, which have been described by several groups.[61,62]

Ligand binding affinity is only one element contributing to the pattern of response to the ligand. The phorbol esters have profound effects on gene expression,[63] including the induction of elevated levels of phorbol ester targets such as PKCα or RasGRP3.[61] They also have profound effects on PKC stability, often leading to downregulation.[64] Importantly, bryostatin 1 shows substantial differences from the phorbol esters in the pattern of PKC isoform downregulation that it induces.[44,61,65] PKCα and PKCβ tend to be more rapidly downregulated. PKCδ shows biphasic downregulation, with protection at high bryostatin 1 concentrations. PKCε is relatively resistant to downregulation. Here we report that Munc13-1 protein levels become elevated after treatment with bryostatin 1 for 24 h, further supporting the concept that bryostatin 1 could enhance vesicle priming, through its direct action on Munc13-1 and on its effect to increase Munc13-1 levels.

In mouse brain, Munc13-1 is predominantly expressed in the hippocampus where it accounts for 90% of the glutamatergic synapses.[25,43] Additionally, activation of Munc13-1 has been shown to increase synaptic activity and could potentially rescue hippocampal glutamatergic neurons from irregular episodes of long-term depression and promote synaptic integrity. In glutamatergic hippocampal neurons, neurodegenerative conditions result in dysfunctional synaptic activity that affects cycles of normal potentiation and depression.[66,67] Under such synaptotoxic conditions, including oxidative stress or the presence of toxic protein aggregates, these irregular synaptic cycles likely result in aberrant episodes of long-term depression that cause axonal shrinkage and loss of dendritic spines.[67,68] Under these stringent neuronal conditions, presynaptic proteins that function to increase synaptic activity could serve as targets for improving synapse integrity and reducing the loss of neuronal connections. On the basis of our findings, together with the location of Munc13 isoform expression and their essential role in neuronal transmission, Munc13 isoforms may serve as potential molecular targets to prevent the loss of synapses in hippocampal neurons and thereby mitigate the cognitive deficits of neurodegenerative diseases. Ultimately, studies exploring the neuroprotective properties of bryostatin 1

DOI: 10.1021/acs.biochem.9b00427
Biochemistry 2019, 58, 3016−3030

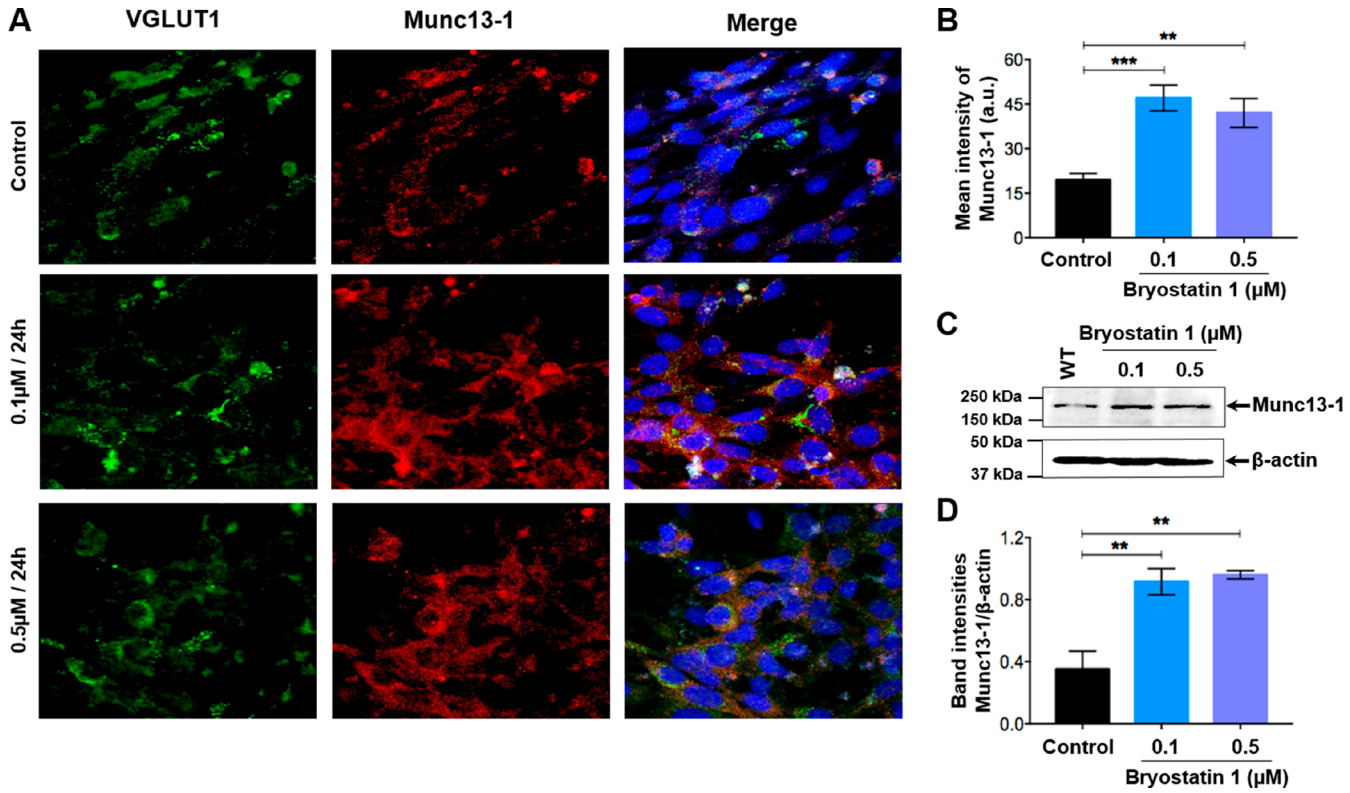

Figure 10. Bryostatin 1 induces Munc13-1 expression in HT22 cells. Differentiated HT22 cells were treated with either 0.1 or 0.5 μM bryostatin 1 for 24 h. (A) Double-label immunocytochemistry of VGLUT1 (glutamatergic neuron marker) in green and Munc13-1 in red. Nuclear staining with DAPI, present only in the merged images, is colored blue. (B) Quantification of the mean intensity of Munc13-1 expression in the cytosol of HT22 cells. (C) Representative Western blot illustrating the expression of Munc13-1 in differentiated HT22 cells. (D) Bar graph showing quantitative densitometric analysis of the Munc13-1:β-actin ratio in HT22 cells. Six different regions from each coverslip per experimental group were imaged, and 20−40 cells from each field were counted. Data are means ± SEM of two or three independently performed experiments. ***P < 0.001, and **P < 0.01. Data were analyzed by two-way ANOVA with Tukey's multiple-comparison test.

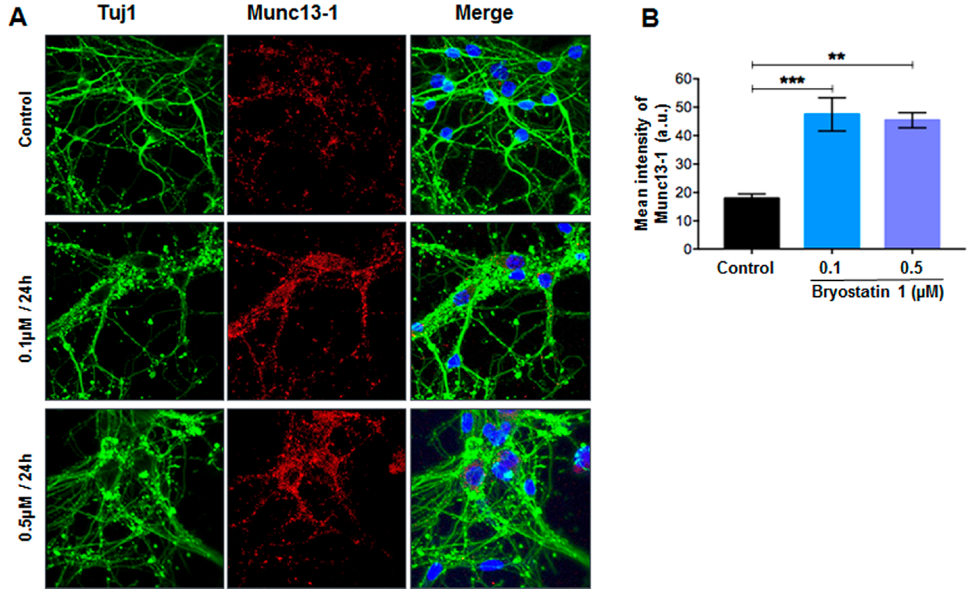

Figure 11. Bryostatin 1 induces Munc13-1 expression in primary hippocampal neurons. Primary hippocampal neurons were treated with either 0.1 or 0.5 μM bryostatin 1 for 24 h. (A) Double-label immunocytochemistry of Tuj-1 (green) and Munc13-1 (red) in primary hippocampal neurons. Nuclear staining, present only in the merged images, is colored blue. (B) Quantification of the mean intensity of Munc13-1 expression in the cytosol of primary hippocampal neurons. Six different regions from each coverslip per experimental group were imaged, and 10−20 cells from each field were counted. Data are means ± SEM of two or three independently performed experiments. ***P < 0.001, and **P < 0.01. Data were analyzed by one-way ANOVA with Tukey's multiple-comparison test.

DOI: 10.1021/acs.biochem.9b00427
Biochemistry 2019, 58, 3016−3030

should be further explored in terms of Munc13 modulation along with that of PKCs.

Of course, it is important to remember that the bryostatins, like the phorbol esters, also target other neuronally relevant signaling proteins, such as the chimaerins and RasGRPs, and their actions at the organismal level will reflect the time-dependent integral of their actions on all of their relevant targets.

■ ASSOCIATED CONTENT

Supporting Information

The Supporting Information is available free of charge on the ACS Publications website at DOI: 10.1021/acs.biochem.9b00427.

Binding of bryostatin 1 to the Munc13-1 C1 domain and its W588A mutant and effect of PMA and bryostatin 1 on bMunc13-2 membrane translocation (PDF)

Accession Codes

Q62768, Q62769, NP_074053, and P28867.

■ AUTHOR INFORMATION

Corresponding Author

*Department of Pharmacological and Pharmaceutical Sciences, Health 2, 4849 Calhoun Rd., Room 3044, Houston, TX 77204-5037. E-mail: jdas@uh.edu. Telephone: 713-743-1708. Fax: 713-743-1229.

ORCID

Anamitra Ghosh: 0000-0001-9740-2070

Joydip Das: 0000-0003-1540-5804

Present Address

§A.G.: Baylor College of Medicine, One Baylor Plaza, Houston, TX 77030.

Author Contributions

F.A.B. and A.C. contributed equally to this work. J.D., N.K., and P.M.B. designed the study. F.A.B., J.D., S.P., N.K., Y.Y., and P.M.B. wrote the paper. A.C., F.A.B., S.P., and N.K. performed cell culture and confocal studies. N.K. and G.A.M. measured the radioactive binding. Y.Y. did the modeling, and A.G. performed the neuronal culture studies.

Funding

This research was supported in part by the Intramural Research Program, National Institutes of Health, Center for Cancer Research, National Cancer Institute (Project Z1A BC 005270), and by Grant 1R01 AA022414-01A1 to J.D.

Notes

The authors declare no competing financial interest.

■ ACKNOWLEDGMENTS

The authors thank Dr. N. Brose of the Max Planck Institute for Experimental Medicine for providing us with the constructs for Munc13-1 and Munc13-2. The authors thank Dr. J. L. Leasure for assistance with the animal experiments.

■ REFERENCES

(1) Pettit, G. R. (1991) The Bryostatins. In *Fortschritte der Chemie organischer Naturstoffe/Progress in the Chemistry of Organic Natural Products* (Herz, W., Kirby, G. W., Steglich, W., and Tamm, C., Eds.) pp 153−195, Springer, Vienna.

(2) Mutter, R., and Wills, M. (2000) Chemistry and clinical biology of the bryostatins. *Bioorg. Med. Chem. 8*, 1841−1860.

(3) Yi, P., Schrott, L., Castor, T. P., and Alexander, J. S. (2012) Bryostatin-1 vs. TPPB: dose-dependent APP processing and PKC-alpha, -delta, and -epsilon isoform activation in SH-SY5Y neuronal cells. *J. Mol. Neurosci. 48*, 234−244.

(4) Ruan, B. F., and Zhu, H. L. (2012) The chemistry and biology of the bryostatins: potential PKC inhibitors in clinical development. *Curr. Med. Chem. 19*, 2652−2664.

(5) Sun, M. K., and Alkon, D. L. (2006) Bryostatin-1: pharmacology and therapeutic potential as a CNS drug. *CNS Drug Rev. 12*, 1−8.

(6) Sun, M. K., Hongpaisan, J., Lim, C. S., and Alkon, D. L. (2014) Bryostatin-1 restores hippocampal synapses and spatial learning and memory in adult fragile x mice. *J. Pharmacol. Exp. Ther. 349*, 393−401.

(7) Farlow, M. R., Thompson, R. E., Wei, L. J., Tuchman, A. J., Grenier, E., Crockford, D., Wilke, S., Benison, J., and Alkon, D. L. (2019) A Randomized, Double-Blind, Placebo-Controlled, Phase II Study Assessing Safety, Tolerability, and Efficacy of Bryostatin in the Treatment of Moderately Severe to Severe Alzheimer's Disease. *J. Alzheimer's Dis. 67*, 555−570.

(8) Schrott, L. M., Jackson, K., Yi, P., Dietz, F., Johnson, G. S., Basting, T. F., Purdum, G., Tyler, T., Rios, J. D., Castor, T. P., and Alexander, J. S. (2015) Acute oral Bryostatin-1 administration improves learning deficits in the APP/PS1 transgenic mouse model of Alzheimer's disease. *Curr. Alzheimer Res. 12*, 22−31.

(9) Nelson, T. J., Sun, M. K., Lim, C., Sen, A., Khan, T., Chirila, F. V., and Alkon, D. L. (2017) Bryostatin Effects on Cognitive Function and PKCvarepsilon in Alzheimer's Disease Phase IIa and Expanded Access Trials. *J. Alzheimer's Dis. 58*, 521−535.

(10) Safaeinejad, F., Bahrami, S., Redl, H., and Niknejad, H. (2018) Inhibition of Inflammation, Suppression of Matrix Metalloproteinases, Induction of Neurogenesis, and Antioxidant Property Make Bryostatin-1 a Therapeutic Choice for Multiple Sclerosis. *Front. Pharmacol. 9*, 625.

(11) Kortmansky, J., and Schwartz, G. K. (2003) Bryostatin-1: a novel PKC inhibitor in clinical development. *Cancer Invest. 21*, 924−936.

(12) Das, J., and Rahman, G. M. (2014) C1 domains: structure and ligand-binding properties. *Chem. Rev. 114*, 12108−12131.

(13) Newton, A. C. (2001) Protein kinase C: structural and spatial regulation by phosphorylation, cofactors, and macromolecular interactions. *Chem. Rev. 101*, 2353−2364.

(14) Irie, K., Nakagawa, Y., and Ohigashi, H. (2004) Indolactam and benzolactam compounds as new medicinal leads with binding selectivity for C1 domains of protein kinase C isozymes. *Curr. Pharm. Des. 10*, 1371−1385.

(15) Nakagawa, Y., Yanagita, R. C., Hamada, N., Murakami, A., Takahashi, H., Saito, N., Nagai, H., and Irie, K. (2009) A simple analogue of tumor-promoting aplysiatoxin is an antineoplastic agent rather than a tumor promoter: development of a synthetically accessible protein kinase C activator with bryostatin-like activity. *J. Am. Chem. Soc. 131*, 7573−7579.

(16) Lai, Y., Choi, U. B., Leitz, J., Rhee, H. J., Lee, C., Altas, B., Zhao, M., Pfuetzner, R. A., Wang, A. L., Brose, N., Rhee, J., and Brunger, A. T. (2017) Molecular Mechanisms of Synaptic Vesicle Priming by Munc13 and Munc18. *Neuron 95*, 591−607.

(17) He, E., Wierda, K., van Westen, R., Broeke, J. H., Toonen, R. F., Cornelisse, L. N., and Verhage, M. (2017) Munc13−1 and Munc18−1 together prevent NSF-dependent de-priming of synaptic vesicles. *Nat. Commun. 8*, 15915.

(18) Rodarte, E. M., Ramos, M. A., Davalos, A. J., Moreira, D. C., Moreno, D. S., Cardenas, E. I., Rodarte, A. I., Petrova, Y., Molina, S., Rendon, L. E., Sanchez, E., Breaux, K., Tortoriello, A., Manllo, J., Gonzalez, E. A., Tuvim, M. J., Dickey, B. F., Burns, A. R., Heidelberger, R., and Adachi, R. (2018) Munc13 proteins control regulated exocytosis in mast cells. *J. Biol. Chem. 293*, 345−358.

(19) Sakamoto, H., Ariyoshi, T., Kimpara, N., Sugao, K., Taiko, I., Takikawa, K., Asanuma, D., Namiki, S., and Hirose, K. (2018) Synaptic weight set by Munc13−1 supramolecular assemblies. *Nat. Neurosci. 21*, 41−49.

DOI: 10.1021/acs.biochem.9b00427
Biochemistry 2019, 58, 3016−3030

(20) Betz, A., Ashery, U., Rickmann, M., Augustin, I., Neher, E., Sudhof, T. C., Rettig, J., and Brose, N. (1998) Munc13−1 is a presynaptic phorbol ester receptor that enhances neurotransmitter release. *Neuron 21*, 123−136.
(21) Augustin, I., Betz, A., Herrmann, C., Jo, T., and Brose, N. (1999) Differential expression of two novel Munc13 proteins in rat brain. *Biochem. J. 337* (3), 363−371.
(22) Augustin, I., Korte, S., Rickmann, M., Kretzschmar, H. A., Sudhof, T. C., Herms, J. W., and Brose, N. (2001) The cerebellum-specific Munc13 isoform Munc13−3 regulates cerebellar synaptic transmission and motor learning in mice. *J. Neurosci. 21*, 10−17.
(23) Chen, Z., Cooper, B., Kalla, S., Varoqueaux, F., and Young, S. M., Jr. (2013) The Munc13 proteins differentially regulate readily releasable pool dynamics and calcium-dependent recovery at a central synapse. *J. Neurosci. 33*, 8336−8351.
(24) Yang, Y., and Calakos, N. (2011) Munc13−1 is required for presynaptic long-term potentiation. *J. Neurosci. 31*, 12053−12057.
(25) Augustin, I., Rosenmund, C., Sudhof, T. C., and Brose, N. (1999) Munc13−1 is essential for fusion competence of glutamatergic synaptic vesicles. *Nature 400*, 457−461.
(26) Varoqueaux, F., Sigler, A., Rhee, J. S., Brose, N., Enk, C., Reim, K., and Rosenmund, C. (2002) Total arrest of spontaneous and evoked synaptic transmission but normal synaptogenesis in the absence of Munc13-mediated vesicle priming. *Proc. Natl. Acad. Sci. U. S. A. 99*, 9037−9042.
(27) Ma, C., Li, W., Xu, Y., and Rizo, J. (2011) Munc13 mediates the transition from the closed syntaxin-Munc18 complex to the SNARE complex. *Nat. Struct. Mol. Biol. 18*, 542−549.
(28) Xu, J., Camacho, M., Xu, Y., Esser, V., Liu, X., Trimbuch, T., Pan, Y. Z., Ma, C., Tomchick, D. R., Rosenmund, C., and Rizo, J. (2017) Mechanistic insights into neurotransmitter release and presynaptic plasticity from the crystal structure of Munc13−1 C1C2BMUN. *eLife 6*, e22567.
(29) Lipstein, N., Verhoeven-Duif, N. M., Michelassi, F. E., Calloway, N., van Hasselt, P. M., Pienkowska, K., van Haaften, G., van Haelst, M. M., van Empelen, R., Cuppen, I., van Teeseling, H. C., Evelein, A. M., Vorstman, J. A., Thoms, S., Jahn, O., Duran, K. J., Monroe, G. R., Ryan, T. A., Taschenberger, H., Dittman, J. S., Rhee, J. S., Visser, G., Jans, J. J., and Brose, N. (2017) Synaptic UNC13A protein variant causes increased neurotransmission and dyskinetic movement disorder. *J. Clin. Invest. 127*, 1005−1018.
(30) Kapfhamer, D., Bettinger, J. C., Davies, A. G., Eastman, C. L., Smail, E. A., Heberlein, U., and McIntire, S. L. (2008) Loss of RAB-3/A in Caenorhabditis elegans and the mouse affects behavioral response to ethanol. *Genes, Brain Behav. 7*, 669−676.
(31) Giovedi, S., Darchen, F., Valtorta, F., Greengard, P., and Benfenati, F. (2004) Synapsin is a novel Rab3 effector protein on small synaptic vesicles. II. Functional effects of the Rab3A-synapsin I interaction. *J. Biol. Chem. 279*, 43769−43779.
(32) Cosen-Binker, L. I., Lam, P. P., Binker, M. G., Reeve, J., Pandol, S., and Gaisano, H. Y. (2007) Alcohol/cholecystokinin-evoked pancreatic acinar basolateral exocytosis is mediated by protein kinase C alpha phosphorylation of Munc18c. *J. Biol. Chem. 282*, 13047−13058.
(33) Ikin, A. F., Causevic, M., Pedrini, S., Benson, L. S., Buxbaum, J. D., Suzuki, T., Lovestone, S., Higashiyama, S., Mustelin, T., Burgoyne, R. D., and Gandy, S. (2007) Evidence against roles for phorbol binding protein Munc13−1, ADAM adaptor Eve-1, or vesicle trafficking phosphoproteins Munc18 or NSF as phospho-state-sensitive modulators of phorbol/PKC-activated Alzheimer APP ectodomain shedding. *Mol. Neurodegener. 2*, 23.
(34) Nonet, M. L., Staunton, J. E., Kilgard, M. P., Fergestad, T., Hartwieg, E., Horvitz, H. R., Jorgensen, E. M., and Meyer, B. J. (1997) Caenorhabditis elegans rab-3 mutant synapses exhibit impaired function and are partially depleted of vesicles. *J. Neurosci. 17*, 8061−8073.
(35) Bosco, D. A., and Landers, J. E. (2010) Genetic determinants of amyotrophic lateral sclerosis as therapeutic targets. *CNS Neurol. Disord.: Drug Targets 9*, 779−790.
(36) Su, X. W., Broach, J. R., Connor, J. R., Gerhard, G. S., and Simmons, Z. (2014) Genetic heterogeneity of amyotrophic lateral sclerosis: implications for clinical practice and research. *Muscle Nerve 49*, 786−803.
(37) Finsterer, J., and Burgunder, J. M. (2014) Recent progress in the genetics of motor neuron disease. *Eur. J. Med. Gene. 57*, 103−112.
(38) Diekstra, F. P., Van Deerlin, V. M., van Swieten, J. C., Al-Chalabi, A., Ludolph, A. C., Weishaupt, J. H., Hardiman, O., Landers, J. E., Brown, R. H., Jr., van Es, M. A., Pasterkamp, R. J., Koppers, M., Andersen, P. M., Estrada, K., Rivadeneira, F., Hofman, A., Uitterlinden, A. G., van Damme, P., Melki, J., Meininger, V., Shatunov, A., Shaw, C. E., Leigh, P. N., Shaw, P. J., Morrison, K. E., Fogh, I., Chio, A., Traynor, B. J., Czell, D., Weber, M., Heutink, P., de Bakker, P. I., Silani, V., Robberecht, W., van den Berg, L. H., and Veldink, J. H. (2014) C9orf72 and UNC13A are shared risk loci for amyotrophic lateral sclerosis and frontotemporal dementia: a genome-wide meta-analysis. *Ann. Neurol. 76*, 120−133.
(39) Diekstra, F. P., van Vught, P. W., van Rheenen, W., Koppers, M., Pasterkamp, R. J., van Es, M. A., Schelhaas, H. J., de Visser, M., Robberecht, W., Van Damme, P., Andersen, P. M., van den Berg, L. H., and Veldink, J. H. (2012) UNC13A is a modifier of survival in amyotrophic lateral sclerosis. *Neurobiol. Aging 33* (630), 630.e3−630.e8.
(40) Veriepe, J., Fossouo, L., and Parker, J. A. (2015) Neurodegeneration in C. elegans models of ALS requires TIR-1/Sarm1 immune pathway activation in neurons. *Nat. Commun. 6*, 7319.
(41) Yang, X., Wang, S., Sheng, Y., Zhang, M., Zou, W., Wu, L., Kang, L., Rizo, J., Zhang, R., Xu, T., and Ma, C. (2015) Syntaxin opening by the MUN domain underlies the function of Munc13 in synaptic-vesicle priming. *Nat. Struct. Mol. Biol. 22*, 547−554.
(42) Basu, J., Shen, N., Dulubova, I., Lu, J., Guan, R., Guryev, O., Grishin, N. V., Rosenmund, C., and Rizo, J. (2005) A minimal domain responsible for Munc13 activity. *Nat. Struct. Mol. Biol. 12*, 1017−1018.
(43) Brose, N., and Rosenmund, C. (2002) Move over protein kinase C, you've got company: alternative cellular effectors of diacylglycerol and phorbol esters. *J. Cell Sci. 115*, 4399−4411.
(44) Nelson, T. J., and Alkon, D. L. (2009) Neuroprotective versus tumorigenic protein kinase C activators. *Trends Biochem. Sci. 34*, 136−145.
(45) Das, J., Xu, S., Pany, S., Guillory, A., Shah, V., and Roman, G. W. (2013) The pre-synaptic Munc13−1 binds alcohol and modulates alcohol self-administration in Drosophila. *J. Neurochem. 126*, 715−726.
(46) Shen, N., Guryev, O., and Rizo, J. (2005) Intramolecular occlusion of the diacylglycerol-binding site in the C1 domain of munc13−1. *Biochemistry 44*, 1089−1096.
(47) Kazanietz, M. G., Lewin, N. E., Bruns, J. D., and Blumberg, P. M. (1995) Characterization of the cysteine-rich region of the Caenorhabditis elegans protein Unc-13 as a high affinity phorbol ester receptor. Analysis of ligand-binding interactions, lipid cofactor requirements, and inhibitor sensitivity. *J. Biol. Chem. 270*, 10777−10783.
(48) Irie, K., Masuda, A., Shindo, M., Nakagawa, Y., and Ohigashi, H. (2004) Tumor promoter binding of the protein kinase C C1 homology domain peptides of RasGRPs, chimaerins, and Unc13s. *Bioorg. Med. Chem. 12*, 4575−4583.
(49) Pany, S., You, Y., and Das, J. (2016) Curcumin Inhibits Protein Kinase Calpha Activity by Binding to Its C1 Domain. *Biochemistry 55*, 6327−6336.
(50) Pany, S., Ghosh, A., You, Y., Nguyen, N., and Das, J. (2017) Resveratrol inhibits phorbol ester-induced membrane translocation of presynaptic Munc13−1. *Biochim. Biophys. Acta, Gen. Subj. 1861*, 2640−2651.
(51) Lewin, N. E., and Blumberg, P. M. (2003) [3H]Phorbol 12,13-dibutyrate binding assay for protein kinase C and related proteins. *Methods Mol. Biol. 233*, 129−156.
(52) Das, J., Kedei, N., Kelsey, J. S., You, Y., Pany, S., Mitchell, G. A., Lewin, N. E., and Blumberg, P. M. (2018) Critical Role of Trp-588 of

DOI: 10.1021/acs.biochem.9b00427
Biochemistry 2019, 58, 3016−3030

Presynaptic Munc13−1 for Ligand Binding and Membrane Translocation. *Biochemistry 57*, 732−741.
(53) Cheng, Y., and Prusoff, W. H. (1973) Relationship between the inhibition constant (K1) and the concentration of inhibitor which causes 50% inhibition (I50) of an enzymatic reaction. *Biochem. Pharmacol. 22*, 3099−3108.
(54) Morris, G. M., Huey, R., Lindstrom, W., Sanner, M. F., Belew, R. K., Goodsell, D. S., and Olson, A. J. (2009) AutoDock4 and AutoDockTools4: Automated docking with selective receptor flexibility. *J. Comput. Chem. 30*, 2785−2791.
(55) Pettit, G. R., Herald, C. L., Doubek, D. L., Herald, D. L., Arnold, E., and Clardy, J. (1982) Isolation and structure of bryostatin 1. *J. Am. Chem. Soc. 104*, 6846−6848.
(56) Pettersen, E. F., Goddard, T. D., Huang, C. C., Couch, G. S., Greenblatt, D. M., Meng, E. C., and Ferrin, T. E. (2004) UCSF Chimera—a visualization system for exploratory research and analysis. *J. Comput. Chem. 25*, 1605−1612.
(57) Leonard, T. A., Rozycki, B., Saidi, L. F., Hummer, G., and Hurley, J. H. (2011) Crystal structure and allosteric activation of protein kinase C betaII. *Cell 144*, 55−66.
(58) Iwig, J. S., Vercoulen, Y., Das, R., Barros, T., Limnander, A., Che, Y., Pelton, J. G., Wemmer, D. E., Roose, J. P., and Kuriyan, J. (2013) Structural analysis of autoinhibition in the Ras-specific exchange factor RasGRP1. *eLife 2*, No. e00813.
(59) Canagarajah, B., Leskow, F. C., Ho, J. Y., Mischak, H., Saidi, L. F., Kazanietz, M. G., and Hurley, J. H. (2004) Structural mechanism for lipid activation of the Rac-specific GAP, beta2-chimaerin. *Cell 119*, 407−418.
(60) Kazanietz, M. G., Lewin, N. E., Gao, F., Pettit, G. R., and Blumberg, P. M. (1994) Binding of [26-3H]bryostatin 1 and analogs to calcium-dependent and calcium-independent protein kinase C isozymes. *Mol. Pharmacol. 46*, 374−379.
(61) Kedei, N., Telek, A., Michalowski, A. M., Kraft, M. B., Li, W., Poudel, Y. B., Rudra, A., Petersen, M. E., Keck, G. E., and Blumberg, P. M. (2013) Comparison of transcriptional response to phorbol ester, bryostatin 1, and bryostatin analogs in LNCaP and U937 cancer cell lines provides insight into their differential mechanism of action. *Biochem. Pharmacol. 85*, 313−324.
(62) Wender, P. A., Hardman, C. T., Ho, S., Jeffreys, M. S., Maclaren, J. K., Quiroz, R. V., Ryckbosch, S. M., Shimizu, A. J., Sloane, J. L., and Stevens, M. C. (2017) Scalable synthesis of bryostatin 1 and analogs, adjuvant leads against latent HIV. *Science 358*, 218−223.
(63) Caino, M. C., von Burstin, V. A., Lopez-Haber, C., and Kazanietz, M. G. (2011) Differential regulation of gene expression by protein kinase C isozymes as determined by genome-wide expression analysis. *J. Biol. Chem. 286*, 11254−11264.
(64) Gould, C. M., and Newton, A. C. (2008) The life and death of protein kinase C. *Curr. Drug Targets 9*, 614−625.
(65) Kedei, N., Telek, A., Czap, A., Lubart, E. S., Czifra, G., Yang, D., Chen, J., Morrison, T., Goldsmith, P. K., Lim, L., Mannan, P., Garfield, S. H., Kraft, M. B., Li, W., Keck, G. E., and Blumberg, P. M. (2011) The synthetic bryostatin analog Merle 23 dissects distinct mechanisms of bryostatin activity in the LNCaP human prostate cancer cell line. *Biochem. Pharmacol. 81*, 1296−1308.
(66) Van Battum, E. Y., Brignani, S., and Pasterkamp, R. J. (2015) Axon guidance proteins in neurological disorders. *Lancet Neurol. 14*, 532−546.
(67) Spires-Jones, T. L., and Hyman, B. T. (2014) The intersection of amyloid beta and tau at synapses in Alzheimer's disease. *Neuron 82*, 756−771.
(68) Shankar, G. M., and Walsh, D. M. (2009) Alzheimer's disease: synaptic dysfunction and Abeta. *Mol. Neurodegener. 4*, 48.

DOI: 10.1021/acs.biochem.9b00427
Biochemistry 2019, 58, 3016−3030